

Synchronization for Variable Data Rate LEO Direct-to-Earth Optical Links

Giulio Colavolpe

Dept. of Engineering and Architecture
University of Parma
and CNIT Research Unit
43124 Parma, Italy
ORCID 0000-0002-0577-8626

Tommaso Foggi

Dept. of Engineering and Architecture
University of Parma
and CNIT Research Unit
43124 Parma, Italy
ORCID 0000-0003-1747-3130

Armando Vannucci

Dept. of Engineering and Architecture
University of Parma
and CNIT Research Unit
43124 Parma, Italy
ORCID 0000-0002-5939-4134

Abstract—The recent developments in the field of direct-to-Earth (DTE) for low-Earth-orbit (LEO) satellite optical links have shown the potential benefits of on-off-keying-based communications with the variable data rate (VDR) technique, in contrast to the traditional constant data rate (CDR) approach. In this paper, relevant link level aspects are analyzed, namely: time, frame, and amplitude synchronization, showing that reliable and performing techniques allow to fully exploit the advantages offered by the VDR strategy.

Index Terms—Free Space Optics; Low Earth Orbit satellite communications; Variable Data Rate.

I. INTRODUCTION

In recent years, new commercial missions resorting to optical links have emerged, as the European data relay system (EDRS) [1], and low Earth orbits (LEO), direct-to-Earth (DTE) optical communications can potentially have a significant application in such field [2].

Currently flying and planned optical LEO-DTE systems transmit at a constant data rate (CDR) while passing over an optical ground station (OGS) [3], without taking into account the characteristics of the propagation channel that typically vary significantly during the satellite pass. Free space loss, atmospheric attenuation, and turbulence of the atmosphere's refractive index show a strong dependence on the satellite elevation angle [4], the latter causing fading due to scintillation [5]. The CDR transmission mode trades between a high transmission data rate, for a short duration, and a long satellite visibility window, at low rates.

Instead, a variable data rate (VDR) approach aims at reducing the performance gap with respect to the channel capacity and, at the same time, allows a longer visibility window. This can be achieved by splitting the pass of the LEO satellite into predefined sectors, and optimizing the data rate in each of them. In particular, in the next generation of Copernicus missions, the VDR concept is based on the variation of the modulation order and of the rate of the forward error correcting (FEC) code [6]. However, in typical optical

The work of G. Colavolpe has been supported by MIUR under the PRIN Liquid-Edge contract; T. Foggi and A. Vannucci acknowledge the financial support of the European Space Agency (ESA) under contract n. 4000130204/20/NL/FE.

LEO-DTE waveforms, such as the one currently defined by the Consultative Committee for Space Data Systems (CCSDS) Optical Working group, the modulation is fixed.

The focus of this paper is on LEO downlink, with a small ground telescope and a low cost receiver without adaptive optics (AO). Thus, we put emphasis on waveform design and receiver synchronization. The expected benefit in terms of throughput has already been forecast in previous works, mostly under ideal conditions and irrespective of the technological implementation [7]. In this paper, the implementation of VDR in optical LEO-DTE on-off keying (OOK) waveforms is proposed by relying on the spreading of data, i.e., the transmission at a fixed chip rate (hence, with a fixed receiver bandwidth) and adapting the data rate by repeating/spreading each data symbol by a desired factor. The proposed approach requires only digital baseband operations so that the front-end hardware is not sensitive to the adopted spreading factor. We assess its performance by numerical simulations with respect to synchronization issues and to the achievable receiver sensitivity.

II. GENERAL DESIGN ASPECTS

We consider a free space optical (FSO) communication system employing the OOK modulation and assume that the receiver employs an avalanche photo-diode (APD), so that both thermal and shot noise have to be considered. The received signal after the APD can thus be expressed as

$$r(t) = h \sum_k a_k p(t - kT - t_0) + w(t - t_0), \quad (1)$$

where the two terms in (1) are the useful signal and the noise process at the receiver, both affected by an unknown delay t_0 introduced by the channel. In (1), $\mathbf{a} = \{a_k\}$ is the sequence of binary transmitted symbols ($a_k \in \{0, 1\}$), T is the symbol time, and h is typically an unknown amplitude, accounting for the random nature of the channel. We consider a non-return-to-zero (NRZ) transmission, with a unit-energy rectangular shaping pulse $p(t)$.

The noise process $w(t)$ in (1) can be expressed as

$$w(t) = w_{\text{th}}(t) + w_{\text{sh}}(t) \sqrt{T} \sum_k a_k p(t - kT), \quad (2)$$

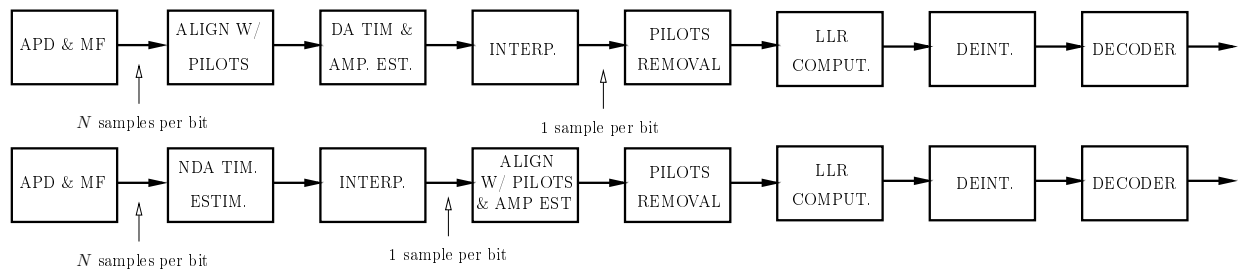


Fig. 1. Receiver architecture for DA (top) or NDA (bottom) timing synchronization.

i.e., as the sum of the thermal noise $w_{th}(t)$, with two-sided power spectral density (PSD) $N_0/2$, and of the independent shot noise $w_{sh}(t)$, with two-sided PSD $N_{sh}/2$ (possibly depending on h), both assumed to be white and Gaussian.

In order to perform synchronization, as well as to estimate the value of h , we resort to data-aided (DA) estimation, hence we assume that blocks of pilot symbols are periodically inserted in the transmitted data stream.

The unknown delay t_0 in (1) can be expressed as $t_0 = k_0T + \tau$, so that its estimation is performed in two steps, whose order depends on the chosen receiver architecture. In the *frame synchronization* step, the estimation of k_0 is performed by exploiting proper fields of known symbols. In the other step, a *timing synchronization* algorithm has instead the task of estimating the residual fractional delay τ .

At the transmitter, the codewords at the output of a FEC channel encoder are interleaved, since atmospheric turbulence is a slowly varying phenomenon with a very long coherence time. Pilot fields are then inserted and the resulting bit stream is modulated using an OOK modulation with NRZ pulses.

The corresponding receiver architecture is reported in Fig. 1 (top). After the APD, we assume that a matched filter (MF) is present, where N samples per symbol are extracted and processed at its output. *Frame synchronization* is performed first, by searching the correct alignment with the pilot fields. *DA timing synchronization* is performed next, together with the estimation of the unknown amplitude h . The signal is then downsampled to one sample per symbol, by using interpolation. After pilot removal, the log-likelihood ratios are computed, deinterleaved, and passed to the decoder.

As an alternative, we also consider a different receiver architecture, shown in Fig. 1 (bottom), in which timing synchronization is performed in closed-loop non-data-aided (NDA) mode, prior to any other receiver function. After timing synchronization and interpolation, the remaining functions are performed by using only one sample per symbol, i.e., frame synchronization is performed jointly with amplitude estimation in DA mode. After that, pilot removal, log-likelihood ratios computation, deinterleaving, and decoding are performed, as in the DA case.

Suppose to observe a chunk of the continuous-time received signal (1), with support $[\tilde{t}_0, \tilde{t}_0 + LT]$, where L is the length of the pilot sequence. The value \tilde{t}_0 is a tentative value of the actual channel delay t_0 , that is assumed by the receiver and

can be expressed as $\tilde{t}_0 = \tilde{k}_0T + \tilde{\tau}$. We assume that the symbols in the observation window are known, as is the thermal noise PSD. On the contrary, the amplitude h is unknown and will be jointly estimated with timing; its tentative value at the receiver is denoted by \tilde{h} . In the low-power regime, at which we expect the receiver to operate, thermal noise dominates over shot noise. Under the assumption that the shot noise is negligible, the likelihood function for the joint estimation of t_0 and h , is [8]

$$\Lambda(\tilde{t}_0, \tilde{h}) = \tilde{h} \sum_{k=0}^{L-1} a_k x(kT + \tilde{t}_0) - \frac{1}{2} \tilde{h}^2 \sum_{k=0}^{L-1} a_k^2, \quad (3)$$

where

$$x(t) = \frac{1}{\sqrt{T}} \int_t^{t+T} r(\alpha) d\alpha = h \sum_k a_k g(t - kT - t_0) + n(t - t_0) \quad (4)$$

is the signal at the output of the MF. More precisely, $n(t - t_0)$ is the filtered noise while $g(t)$ is the triangular autocorrelation function of the rectangular transmission pulse $p(t)$.

By defining the set of indices $\mathcal{K}_1 = \{k \in \{0, 1, 2, \dots, L-1\} : a_k = 1\}$, corresponding to bits “1” in the sequence of L known symbols, and by $K_1 = |\mathcal{K}_1|$ their total number, we can define

$$\Gamma(\tilde{k}_0, \tilde{\tau}) = \sum_{k \in \mathcal{K}_1} x(\tilde{k}_0T + kT + \tilde{\tau}), \quad (5)$$

as the sum over \mathcal{K}_1 of samples at the matched filter output, with symbol spacing and with a tentative delay $\tilde{t}_0 = \tilde{k}_0T + \tilde{\tau}$. This way, (3) can be compactly expressed as $\Lambda(\tilde{t}_0, \tilde{h}) = \tilde{h} \Gamma(\tilde{k}_0, \tilde{\tau}) - \frac{1}{2} \tilde{h}^2 K_1$, and its maximum over the possible values of the delay is achieved by estimating k_0 and τ as $(\hat{k}_0, \hat{\tau}) = \text{argmax}_{\tilde{k}_0, \tilde{\tau}} \Gamma(\tilde{k}_0, \tilde{\tau})$ (where we constrain $\hat{\tau}$ in an interval with duration T) and by the estimate that follows for the attenuation, $\hat{h} = \Gamma(\hat{k}_0, \hat{\tau}) / K_1$.

After the MF, N specific values $\tilde{\tau} + \tilde{n} \frac{T}{N}$ (with $\tilde{n} \in \{0, 1, \dots, N-1\}$) are considered at the receiver. The frame synchronization step of the algorithm consists in the identification of the maximum of Γ in a sliding window fashion. The metric Γ is computed according to (5) by using L samples with spacing T . The grid of L samples is then shifted in time by T/N at every step, by increasing the value considered for \tilde{n} (or otherwise increasing \tilde{k}_0 and resetting \tilde{n} to zero, when $\tilde{n} = N$). Termination is declared when the likelihood function exceeds a properly optimized threshold. A good choice of the pilot

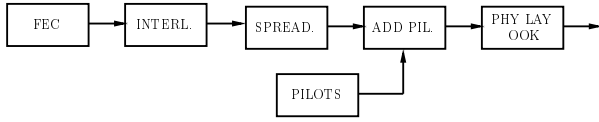


Fig. 2. VDR transmitter.

field symbols is represented by the maximum length sequences or M-sequences [9], thanks to their autocorrelation properties. Obviously, the miss-detection probability can be reduced by increasing the length L of the M-sequence.

The frame synchronization step also yields a coarse timing estimate $\tau_1 = \tilde{\tau} + \hat{n} \frac{T}{N}$. If the frame synchronization is effective, then the residual error lies within a sample interval, and we can define a residual relative error $\varepsilon = (\tau_1 - \tau)/T \in [-1/(2N); 1/(2N)]$. Within this interval, it can be shown that the metrics in (5) can be equivalently expressed as

$$\Gamma(\varepsilon) = h[(K_1 - K_{11})(1 - |\varepsilon|) + K_{11}] + n_1(\varepsilon T), \quad (6)$$

where $n_1(t) = \sum_{k \in \mathcal{K}_1} n(t + kT)$ is the sum of filtered noise samples affecting the “1” symbols and we defined K_{11} as the number of “11” subsequences in the known pilot field. The triangular shape of (6) is related to the triangular autocorrelation $g(t)$ in (4) and, in the absence of noise, hK_1 is its maximum value, at $\varepsilon = 0$, while hK_{11} is its minimum value, at $\varepsilon = \pm 1$, both values being known at the receiver.

Let us shortly denote by $\Gamma_0 = \Gamma(\tilde{k}_0, \tau_1)$ the maximum of the metric in (5) that stems from frame synchronization, corresponding to the estimated start of the frame, and by $\Gamma_{\pm \frac{1}{N}}$ the two neighbouring samples, corresponding to the metric computed at indices $(\tilde{k}_0, \tau_1 \pm \frac{T}{N})$, where $\Gamma_0 > \Gamma_{\pm \frac{1}{N}}$. Given the triangular profile (6) of $\Gamma(\varepsilon)$ and assuming $N \geq 2$ samples per symbol interval, the following linear interpolation yields the maximum of (6),

$$\hat{\varepsilon} = \frac{1}{2N} \frac{\Gamma_{-\frac{1}{N}} - \Gamma_{\frac{1}{N}}}{\Gamma_0 - \min\{\Gamma_{-\frac{1}{N}}, \Gamma_{\frac{1}{N}}\}}, \quad (7)$$

which defines the estimate for the residual relative timing error. Note that in the case of a VDR system, timing estimation via (7) can be accomplished even by using $N = 1$ sample per symbol, provided that proper spreading sequences are employed.

The estimate of τ is finally obtained as $\hat{\tau} = \tau_1 - \hat{\varepsilon}T$, and the maximum of the metric in (6) can be equally expressed in an easy way as $\Gamma_{\max} = \Gamma_0 + \frac{1}{2} \left| \Gamma_{-\frac{1}{N}} - \Gamma_{\frac{1}{N}} \right|$. Finally, the amplitude estimation can be found from the general relationship $\hat{h} = \Gamma_{\max}/K_1$.

The receiver scheme in Fig. 1 (bottom), instead, adopts a NDA timing estimation that is performed first, by implementing one of the traditional algorithms proposed in the literature, as described in Sec. IV. In this case, frame synchronization as well as amplitude estimation can be performed subsequently, after interpolation and downsampling at symbol time.

III. VARIABLE DATA RATE SYSTEM DESIGN

The method proposed to seamlessly change the symbol rate during the satellite pass is to spread the data symbols to the highest possible chip rate the transmit or receive hardware can support. Since both transmitter and receiver always operate at a constant chip rate, the VDR is implemented by changing the spreading factor in each sector of the pass, so that the underlying symbol rate matches the selected symbol rate for each sector. Therefore, the VDR technique foresees the use of spreading sequences to represent the bits “0” and “1”. The chip rate is kept constant whereas the symbol rate is decreased by increasing the length of the spreading sequences. In other words, we may express the transmitted signal as

$$s(t) = \sum_k \sum_{m=0}^{M-1} s_m(a_k) p[t - (kM + m)T_c]$$

where $[s_0(a), s_1(a), \dots, s_{M-1}(a)]^T = \mathbf{s}(a)$ is the spreading sequence associated with bit $a \in \{0, 1\}$, still composed of binary symbols, M is the length of the spreading sequence (here, $M = 2^0, 2^1, 2^2, \dots$), T_c is the chip time, and $p(t)$ is a rectangular pulse with unit energy and duration T_c , i.e.,

$$p(t) = \begin{cases} \frac{1}{\sqrt{T_c}} & 0 \leq t < T_c \\ 0 & \text{otherwise.} \end{cases} \quad (8)$$

We assume perfect synchronization at the receiver. The signal sampled at chip time is used to compute the symbol log-likelihood ratios (LLRS), which are given by the sum of the LLRs associated with each chip, to be sent to the decoder. It follows that the selected spreading sequences, $\mathbf{s}(a)$ and $\mathbf{s}(1 - a)$, should be complementary. Then, it is evident that the performance of these sequences will depend on the number of “1”s and “0”s that they contain, and not on their position. In order to find the best sequences, we looked for the maximization of the mutual information between transmitted symbols and received signal, and, also by exploiting the data processing inequality that allows to express the entropies through the LLRs, we were able to numerically evaluate the mutual information by time averaging.

The conclusion is that for the values of σ_0^2, σ_1^2 , and h at hand, and in the range of values of interest for the average received optical power P_{avg} , we always found that the optimal number M_1 of chips “1” in the spreading sequence corresponding to bit “1” is $M_1 = M$ (or equivalently $M_1 = 0$). The best possible spreading sequences to be associated with bits “0” and “1” are thus $\mathbf{s}(0) = [0, 0, \dots, 0]^T$, $\mathbf{s}(1) = [1, 1, \dots, 1]^T$.

On the other hand, there are different sequences to be preferred from different points of view. As an example, if a NDA timing estimation algorithm is selected, it is more convenient to increase the number of symbol transitions. Thus, from this point of view the best possible spreading sequences are, e.g., $\mathbf{s}(0) = [0, 1, 0, 1, \dots, 0, 1]^T$, $\mathbf{s}(1) = [1, 0, 1, 0, \dots, 1, 0]^T$.

In the following, we will refer to a scheme employing the bit repetition as “scheme 1”, whereas a scheme using the bit alternation will be referred to as “scheme 2”.

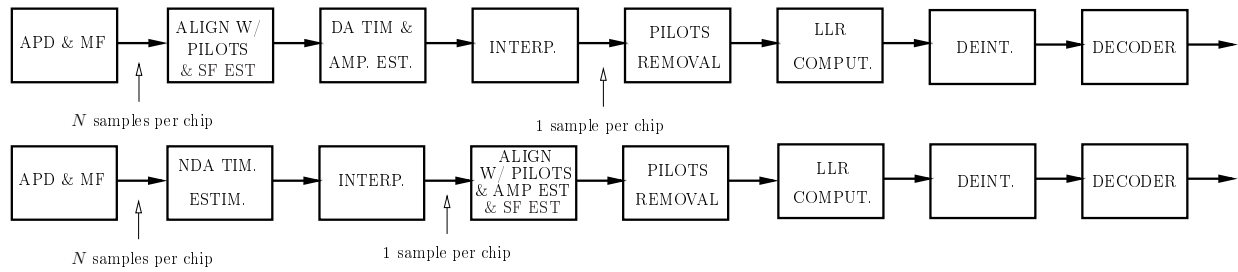


Fig. 3. VDR receiver architecture for DA (top) or NDA (bottom) timing synchronization.

In the case of VDR, the transmitter architecture is depicted in Fig. 2. Compared to the one considered for CDR, the spreading of the coded bits is present. Since the larger the value of M , the lower the value of P_{avg} , it is intuitive that in the case of spreading we will need more pilots to perform a proper estimate of the unknown parameters. On the other hand, if we apply the spreading to the pilot fields too, we could destroy their autocorrelation properties, as discussed in the following.

At the receiver side, we report in Fig.3 two possible architectures for the VDR receiver, either based on DA or NDA timing synchronization; in the first one there is an estimation of the spreading factor (SF), performed jointly with pilot alignment. We assume at most $N = 2$ in the following.

In case of adoption of the NDA architecture, the best choice for the spreading sequence is represented by the “scheme 2”. On the other hand, this spreading sequence, if applied to a pilot field with the aim of obtaining a longer pilot field, will destroy the autocorrelation properties of the M-sequence. As a consequence, in this case it is better to avoid spreading the pilot field. Hence, when the payload is spread by a factor M , we need to adopt a different pilot field with length LM , where L is the length of the pilot field in the absence of spreading.

In a LEO-DTE link, the spreading factor employed will be a deterministic function of the elevation angle. Hence, the OGS can adopt a geometry-based method to predict the employed spreading factor with, at most, an uncertainty between two possible adjacent values, e.g., M and $2M$. The receiver becomes thus aware of the exact spreading factor used by the transmitter by evaluating the correlation with both pilot fields having length M and $2M$. This will allow the receiver to perform both frame synchronization and, implicitly, the estimation of the spreading factor. A possible way to avoid multiple correlations is the adoption of properly designed pilot fields, such that the pilot field with length LM coincides with the first half of the pilot field with length $2LM$.

Let us now consider the DA architecture in Fig. 3 (top). In this case, considering that the different spreading sequences have a limited impact on the BER performance, and since timing synchronization is performed in DA mode using the pilot field, we can generate a longer pilot field by spreading the original pilot field that is used in the absence of spreading. In order to simplify the transmitter, the same spreading sequences can then be used for the payload too. We thus wish to

investigate the impact of different spreading sequences, as applied to obtain a longer pilot field, on DA frame, timing, and amplitude estimation. We shall consider the following scenarios, where a spreading factor M is always assumed and L is the length that was used in the absence of spreading:¹

- **Scenario 1:** longer pilot field by spreading with “scheme 1” the pilot field sequence.
- **Scenario 2:** longer pilot field by spreading with “scheme 2” the pilot field sequence.
- **Scenario 3:** longer pilot field by spreading the pilot field sequence with an M-sequence with length M and its complementary sequence.²
- **Scenario 4:** longer pilot field by using a new M-sequence with length $L' = (L + 1)M - 1$.

The first three schemes show the advantage that different pilot fields do not need to be stored at both transmitter and receiver. In the numerical results that follow we shall compare the four scenarios above.

IV. NUMERICAL RESULTS

When a bit “1” is transmitted, the receiver APD, with responsivity R and multiplication factor M_P , yields an average current equal to $2P_{\text{avg}}RM_P$. The one-sided PSD of thermal noise is $N_0 = i_{\text{th}}^2 = \frac{4kT_0}{R_L}$, where i_{th} is the thermal current density, that is in turn related to the APD’s load resistance R_L and to the receiver temperature T_0 through the Boltzmann’s constant ($k = 1.3806 \cdot 10^{-23}$ J/K). The one-sided PSD of shot noise can be expressed as $N_{\text{sh}} = 4eM_P^2FRP_{\text{avg}}$, where F is the APD excess noise factor and e is the electron charge ($e = 1.60217662 \cdot 10^{-19}$ C). In the numerical results that follow, we use a chip rate of 10 Gchip/s and the following APD parameters: $i_{\text{th}} = 10^{-11}$ A/ $\sqrt{\text{Hz}}$, $F = 5$, $R = 0.9$ A/W, $M_P = 20$.

We first consider the performance of the DA approach. Regarding the performance of frame synchronization, we first considered its evaluation in terms of miss-detection probability, defined as the probability that the timing estimation error exceeds $T/2$, i.e., $P(|\tau - \hat{\tau}| > T/2)$. Fig.4 reports

¹It is worth highlighting that scenarios 3 and 4 were obtained by using M-sequences, which have intrinsically excellent correlation properties, therefore a better performance is expected in terms of miss-detection.

²M-sequences have length $2^P - 1$ with P a proper integer [9]. On the contrary, the spreading factors M are always a power of two. For this reason we appended a bit “0” to the generated M-sequence.

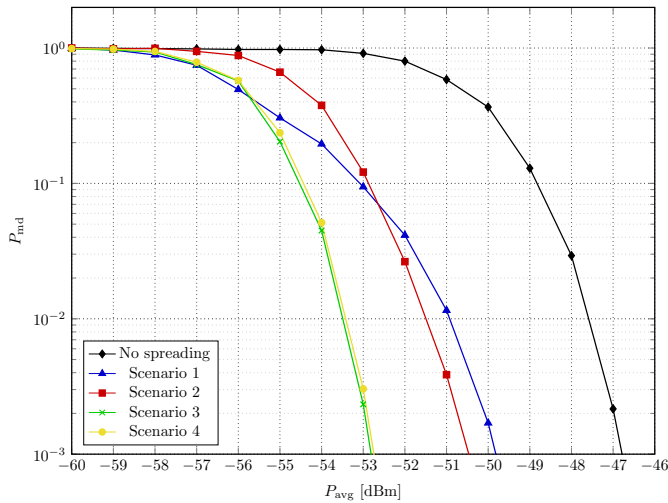


Fig. 4. Miss-detection probability. The original pilot field length is $L = 511$ and the spreading factor is $M = 16$.

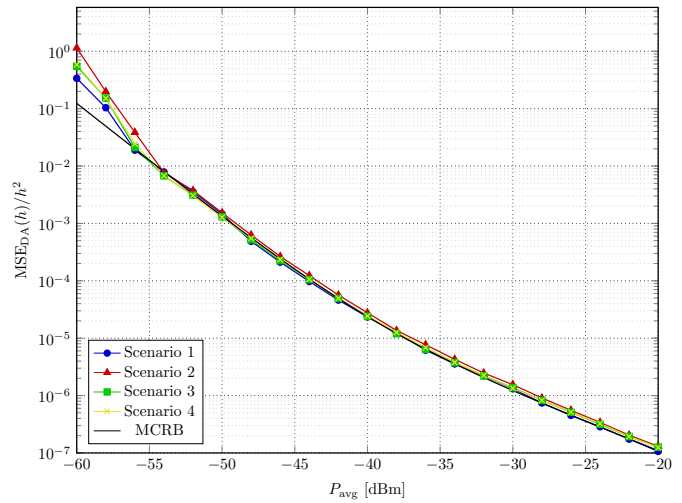


Fig. 6. Performance for amplitude estimation. The spreading factor is $M = 16$.

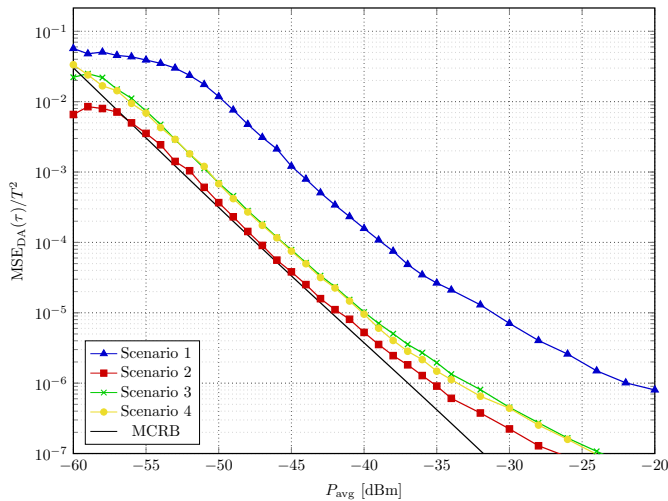


Fig. 5. Performance for timing estimation. The spreading factor is $M = 16$.

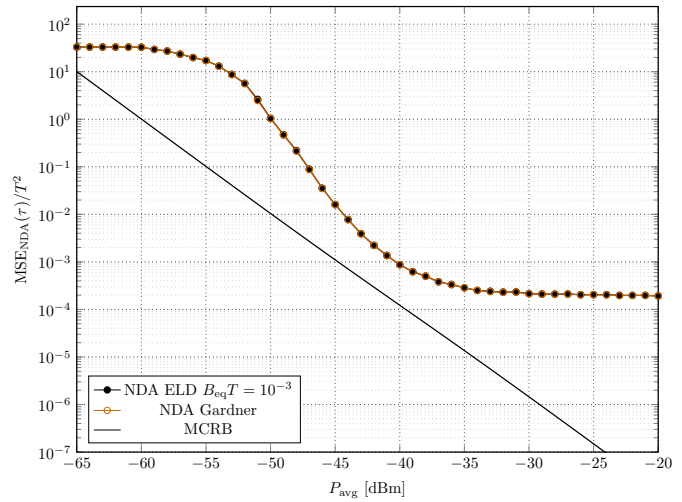


Fig. 7. Performance of the NDA ELD and of the NDA Gardner algorithms for timing estimation in the case of a CDR system ($B_{eq}T = 10^{-3}$).

the results for the proposed algorithm, by first considering a system without any spreading sequence, where a pilot field with length $L = 511$ is employed.³ Performance is compared to that of a VDR system where a spreading factor $M = 16$ is adopted and the four different scenarios described previously are considered for the spreading strategy. A significant gain of more than 6 dB is observed, in scenarios 3 and 4, with respect to the case where no spreading is present. On the other hand, scenario 2 provides the worst performance within the VDR framework. Indeed, in this case the adopted spreading sequences destroy the autocorrelation properties of the M-sequence employed as pilot field, as expected.

Moving to timing synchronization, Fig. 5 reports the estimation results in terms of normalized timing mean squared error

³This means that the spreading was obtained by using a M-sequence with length 15 for scenario 3, and with length $L' = 8191$ for scenario 4 (both with a "0" padded at the end).

(MSE) versus P_{avg} . The four scenarios are again considered in the case of a spreading factor $M = 16$. In this case, scenario 1 is the worst, as expected. Indeed, the number of $0 \rightarrow 1$ and $1 \rightarrow 0$ transitions is the same as in the absence of spreading, so that a spreading gain cannot be expected. On the contrary, scenario 2 is the best one since, in this case, the number of transitions is maximized.

Finally, all four scenarios are equivalent in terms of amplitude estimation, as shown in Fig. 6. As a conclusion, taking into account both timing and frame synchronization, as well as amplitude estimation, scenarios 3 and 4 must be preferred.

If synchronization is instead performed in a NDA fashion, we can consider the simple receiver architecture in Fig. 1 (bottom) for CDR transmission, where timing estimation can be accomplished by traditional NDA algorithms that do not require the knowledge or the estimate of the amplitude h . Fig. 7 shows the performance of two such algorithms in

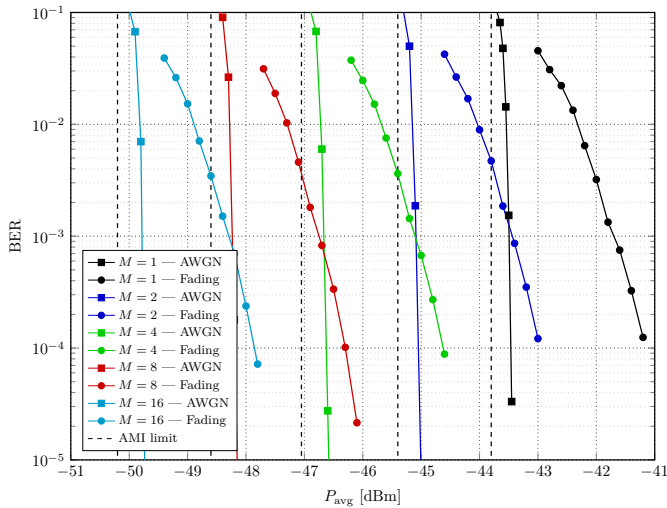


Fig. 8. BER performance on AWGN and turbulent fading channels (PSI=0.1), for a few different spreading factors; SCCC of code rate 0.46 is considered. Results are not sensitive to the adopted spreading scheme.

terms of normalized timing estimation MSE versus P_{avg} . More precisely, the NDA early-late detector (ELD) technique and the NDA technique proposed by Gardner [8] are compared, showing an almost identical performance, when the normalized equivalent bandwidth is set to $B_{\text{eq}}T = 10^{-3}$. Along with simulation results, Figs. 5, 6 and 7 show the modified Cramer-Rao bound (MCRB) computed for the considered system [8], so as to highlight the margin of the achieved performance with respect to the theoretical limit.

As a further step, we analyzed and compared the error rates of CDR and VDR systems, focusing in particular on the impact of the spreading factor M , where $M = 1$ can be seen as a degenerate case of VDR coinciding with a CDR system. We assume perfect synchronization in order to make a fair comparison among different spreading schemes. Fig. 8 reports the BER performance versus P_{avg} , obtained by using a serially concatenated convolutional code (SCCC) with rate 0.46, when employing the two spreading schemes introduced in Sec. III and different values of the spreading factor M . Both an additive white Gaussian noise (AWGN) channel and a channel with stochastic fading due to atmospheric turbulence were considered, where the power scintillation index (PSI), i.e., the normalized variance of h , is equal to 0.1, amounting to weakly turbulent conditions. The theoretical reference of the average mutual information (AMI) for the AWGN scenario, computed by resorting to mutual information numerical evaluation, is also reported. The first result is that, while the two spreading schemes deeply affect DA frame and timing synchronization procedures (as seen above in their related scenarios 1 and 2), they have no real impact on the BER performance, such that the repetition (scheme 1) or alternation (scheme 2) of the information bits produce experimentally identical BER curves; for this reason, a single curve is shown in Fig. 8, for each value of M and channel. Hence, although in principle the spreading sequences can be optimized, in practice the performance gain

this optimization can provide in terms of BER is negligible. This can be theoretically justified by observing the power range in which Fig. 8 was obtained. At the optical power levels of interest, shot noise hardly ever impacts on system performance, so that $\sigma_0^2 \simeq \sigma_1^2$ can be safely assumed. Therefore, the resulting mutual information does not depend on M_1 , so that other spreading schemes could possibly be adopted. For a given average received optical power, it is of course the spreading factor that strongly influences the BER. As expected, the performance scales linearly with the spreading factor. In fact, both for the AWGN and for the turbulent fading channel, a 1.5 dB improvement can be observed on the optical power each time the symbol period, i.e., M , is doubled (while a corresponding improvement by 3 dB would be observed on the electrical signal power, which is proportional to the square of optical power).

V. CONCLUSIONS

The VDR technique addressed in this paper was implemented exclusively at the digital baseband layer and aimed to optimize in a transparent way the data return of optical LEO DTE links by employing OOK with an APD-based receiver, over the whole range of the elevation angle. This was done by investigating and assessing the performance of critical link level aspects, such as receiver synchronization, choice of the spreading sequences, and possible alternative architectures.

ACKNOWLEDGMENT

We gratefully acknowledge the helpful discussions with Pantelis-Daniel Arapoglou and Nicolò Mazzali (ESA-ESTEC).

REFERENCES

- [1] F. Heine, G. Mühlwinkel, H. Zech, S. Philipp-May, and R. Meyer, "The European Data Relay System, high speed laser based data links," in *7th Adv. Sat. Multimedia Systems Conf. and 13th Signal Proc. for Space Comm. Workshop (ASMS/SPSC)*, 2014, pp. 284–286.
- [2] S. Müncheberg, C. Gal, J. Horwath, H. Kinter, L. M. Navajas, and M. Soutullo, "Development status and breadboard results of a laser communication terminal for large LEO constellations," in *Int. Conf. on Space Optics (ICSO)*, vol. 11180. SPIE, 2019, pp. 1180 – 1192.
- [3] C. Fuchs, F. Moll, D. Giggenbach, C. Schmidt, J. Keim, and S. Gaisser, "OSIRISv1 on Flying Laptop: Measurement Results and Outlook," in *IEEE Int. Conf. on Space Optical Systems and Applications (ICSOS)*, 2019.
- [4] F. Moll, "Experimental analysis of channel coherence time and fading behavior in the LEO-ground link," in *Proc. Int. Conf. on Space Optical Systems and Applications (ICSOS)*, Kobe, Japan, May 2014.
- [5] D. Giggenbach and H. Henniger, "Fading-loss assessment in atmospheric free-space optical communication links with on-off keying," *Optical Engineering*, vol. 47, no. 4, 2008.
- [6] N. Toptsidis, P.-D. Arapoglou, and M. Bertinelli, "Link adaptation for Ka band low Earth orbit Earth observation systems: A realistic performance assessment," *International Journal of Satellite Communications and Networking*, vol. 30, no. 3, pp. 131–146, May 2012.
- [7] N. Perlot and T. de Cola, "Throughput maximization of optical leo-ground links," in *Free-Space Laser Communication Technologies XXIV*, H. Hemmati and D. M. Boroson, Eds., vol. 8246, 2012.
- [8] U. Mengali and A. N. D'Andrea, *Synchronization Techniques for Digital Receivers (Applications of Communications Theory)*. Plenum Press, 1997.
- [9] M. Cohn and A. Lempel, "On fast m-sequence transforms," *IEEE Transactions on Information Theory*, vol. 23, pp. 135 – 137, January 1977.